Separation and Purification Technology 220 (2019) 231–237

Contents lists available at ScienceDirect

Separation and Purification Technology

journal homepage: www.elsevier.com/locate/seppur

Layered double hydroxide-modified thin–film composite membranes with remarkably enhanced chlorine resistance and anti-fouling capacity

Peng Lu[a], Wenjun Li[a], Sheng Yang[a], Yi Liu[b,*], Qiang Wang[c], Yanshuo Li[a,*]

[a] School of Materials Science and Chemical Engineering, Ningbo University, 818 Fenghua Road, Ningbo 315211, PR China
[b] State Key Laboratory of Fine Chemicals, School of Chemical Engineering, Dalian University of Technology, 2 Linggong Road, Dalian 116024, PR China
[c] College of Environmental Science and Engineering, Beijing Forestry University, 35 Qinghua East Road, Haidian District, Beijing 100083, PR China

ARTICLE INFO

Keywords:
Layered double hydroxides
Thin–film composite membrane
Chlorine resistance
Anti-fouling

ABSTRACT

Polyamide (PA)-based thin-film composite (TFC) membranes prepared via interfacial polymerization have been widely applied in nanofiltration, reverse osmosis and forward osmosis (FO). However, a major issue facing practical applications of PA-TFC membranes remained the irreversible degradation and fouling of PA upon long-term exposure to aqueous environments. In this study, layered double hydroxides (LDHs) as inorganic additives were incorporated into PA matrices as well as polysulfone (PSf) substrates in attempt to alleviate the membrane degradation and fouling. The effect of location of LDHs on the physicochemical property and separation performance of FO membranes was investigated in detail. Four different FO membranes, including TFC (PA membrane on PSf substrate), TFC-LDH (PA membrane on PSf substrate blended with LDHs), LDH@TFC (LDH post-modified PA membrane on PSf substrate) and LDH@TFC-LDH (LDH post-modified PA membrane on PSf substrate blended with LDHs) were prepared. The water flux followed the sequence TFC-LDH > TFC ≈ LDH@TFC-LDH > LDH@TFC, while the reverse salt flux showed the opposite trend. Moreover, it was observed that compared with pure TFC membrane, not only the surface of LDH@TFC-LDH membrane became more hydrophilic, but also porosity of the substrate became higher, therefore endowing the LDH@TFC-LDH membrane with superior anti-fouling capacity. Moreover, the LDH@TFC-LDH membrane remained stable during long-term chlorination tests under alkaline conditions. To summarize, post-modifying the PA active layer with LDH nanocrystals and blending the PSf substrate with LDH nanocrystals significantly enhanced both anti-fouling capacity and chlorine resistance of prepared membranes without sacrificing the water flux during the FO process.

1. Introduction

Owing to the omission of hydraulic pressure, low fouling propensity and high water recovery rate [1,2], in recent decades forward osmosis (FO) membrane technology has been widely used in desalination [3], food concentration [4], osmotic power generation [5] and wastewater reclamation [2]. However, the major issue hindering its further development remained the serious internal concentration polarization (ICP) in the supporting layer, which had negatively affected the water permeation through prepared FO membrane [6]. ICP phenomenon could induce the formation of undesired boundary layer which could not be completely avoided by simple process optimization [7,8]. Therefore, construction of a supporting layer with higher porosity, lower tortuosity and thinner thickness became indispensable to alleviate the undesired ICP effect [9].

Typically, thin–film composite (TFC) FO membranes consist of ultrathin selective layers (like polyamide (PA)) supported on porous substrates (like polysulfone (PSf)). Unfortunately, PA-TFC membranes may be severely destroyed upon reaction with chlorine (in particular active chlorine species) [10,11]. It should be noted that compared with other pressure-driven membrane separation processes, the fouling of FO membranes was relatively less severe since they could be more conveniently cleaned [12]; nevertheless, fouling remained a great challenge during the application of TFC membranes since the membrane performance may be gradually deteriorated [13]. Therefore, it was imperative for us to improve both the chlorine resistance and anti–-fouling capacity of PA-TFC membranes while simultaneously maintaining a high separation performance.

Recent studies indicated that fabrication of thin-film nanocomposite (TFN) membranes by incorporating inorganic modifiers enabled

* Corresponding authors.
E-mail addresses: diligenliu@dlut.edu.cn (Y. Liu), liyanshuo@nbu.edu.cn (Y. Li).

https://doi.org/10.1016/j.seppur.2019.03.039
Received 17 July 2018; Received in revised form 13 January 2019; Accepted 13 March 2019
Available online 14 March 2019
1383-5866/

significant enhancement of the separation performance of TFC membranes. At present, diverse inorganic modifiers, including TiO_2 [14], SiO_2 [15], zeolite [16], graphene-based materials [17], transition metal dichalcogenides (TMDCs) [18], metal-organic frameworks (MOFs) [19] and layered clays (e.g. Montmorillonite [20] and layered double hydroxides (LDHs) [21]), have been incorporated into porous substrates and proven effective for alleviation of the undesired ICP phenomenon [22,23]. In addition, inorganic modifiers could also be used to decorate PA layers for improving their permselectivity, anti-fouling capacity and chlorine resistance [21].

LDHs, also commonly called hydrotalcite-like compounds, are representative of anionic layered materials composed of positively charged brucite-like 2D sheets, charge compensating anions and solvation molecules located in interlayer galleries [24]. Compositional flexibility and gallery height adjustability give rise to functional diversity. At present, LDHs have found widespread applications in CO_2 adsorption [25], catalysts [26], polymeric modification [27], wastewater treatment [28] and controlled drug delivery [29].

Recent decades witnessed great efforts made in promoting the separation performance of FO membranes relying on LDHs. In our previous studies, LDHs have been used as nanofillers and blended with porous PSf substrates [6]. It was observed that the porosity, pore aperture and surface hydrophilicity were greatly improved. Furthermore, continuous MgAl-CO_3 LDH buffer layers have been coated on polydopamine (PDA)-modified PA active layers for enhancing their chlorine resistance and anti–fouling capacity [21]. Nevertheless, the water flux of prepared LDH-modified TFC membranes was remarkably decreased due to an increased mass transfer barrier [21]. To summarize, previous studies indicated the location of embedded inorganic modifiers within TFC membranes exerted significant influence on their separation performance [1,9]. In this study, we modified PA-TFC membranes with LDHs and systematically investigated the influence of LDHs location on the microstructure, chlorine resistance and anti-fouling capacity of membranes. Moreover, the osmosis performance of both pristine TFC and modified composite membranes were compared. It was observed that simultaneous depositing LDH nanoparticles on the surface of PA active layer and blending the PSf substrate with LDH nanoparticles significantly improved both chlorine resistance and anti–fouling capacity without compromising the water flux.

2. Experimental

2.1. Materials

PSf (Mn: 22,000 Da) and polydopamine (PDA, 98.5%) were purchased from Sigma-Aldrich. Polyester non-woven fabric (PET, grade 3249) was provided by Ahlstrom (Helsinki, Finland). 1,3-phenylenediamine (MPD, > 99%) and 1,3,5-benzenetricarbonyl trichloride (TMC, ~98%) were purchased from TCI Chemicals Ltd. 1-methyl-2-pyrrolidinone (NMP, anhydrous, ~99.5%), *N,N*-di-methylformamide (DMF, anhydrous, ~99.8%), $Mg(NO_3)_2{\cdot}6H_2O$, $Al(NO_3)_3{\cdot}9H_2O$, NaOH, HCl, NaCl, Na_2CO_3, sodium alginate, NaClO (available chlorine 8–12%) and $NaHSO_3$ were purchased from Sinopharm Chemical Reagent Co., Ltd. Deionized (DI) water utilized in membrane performance tests was obtained from Milli-Q ultrapure water purification system (Millipore, Billerica, MA).

2.2. Synthesis of LDH nanoparticles

MgAl-CO_3 LDH nanoparticles (ca. 20–30 nm) were obtained by a co-precipitation method as described in our previous work [6,21]. First, 9.6 g $Mg(NO_3)_2{\cdot}6H_2O$ and 4.7 g $Al(NO_3)_3{\cdot}9H_2O$ were added in 50 ml DI water as solution A, and 2.65 g Na_2CO_3 was added in 50 ml DI water as solution B. Second, solution A was added drop-wise to solution B while maintaining a pH value of 12 via controlled addition of 4 M NaOH solution. Third, the precursor solution was aged for 12 h under continuous stirring at room temperature (RT). Finally, solid precipitates were washed with copious of DI-water and ready for use [21]. It should be emphasized that washing with acetone was indispensable to prevent their further agglomeration [30].

2.3. Preparation of PSf-LDH composite substrates

Pure PSf substrates were fabricated with the conventional non-solvent induced phase inversion method. PSf-LDH composite substrates were prepared as follows: First, given amount of MgAl-CO_3 LDH nanoparticles was added to 88 g solvent (mass ratio of NMP/DMF = 3/1) and subjected to ultrasonication for 30 min to minimize nanoparticles agglomeration. Second, 12 g PSf powders were dissolved in above precursor solution and subjected to magnetic stirring for 12 h and deaeration for another 8 h at RT. Third, resultant solutions were casted on a wetted PET fabric with a 150 μm casting knife (Elcometer 3530). Finally, fresh substrates were immediately immersed in a precipitation bath containing 3 wt% NMP solution for 10 min at RT and then stored in a DI water bath for at least 24 h prior to use as substrates.

2.4. Preparation of PA active layer and LDH-modified PA active layer

Pure PA active layers were prepared by interfacial polymerization reaction on porous PSf substrates. First, the PSf substrate was immersed in 3.4 wt% MPD solution for 2 min, and an air knife was used to remove excess MPD solution. In the next step, the MPD-modified substrate was immersed into an Isopar-G solution containing 0.15 wt% TMC for 1 min. Consequently, the membrane was cured in DI water at 95 °C for 2 min, successively rinsed with 200 ppm NaOCl and 1000 ppm $NaHSO_3$ aqueous solution for 2 and 0.5 min, respectively. Finally, fresh TFC membrane was thoroughly rinsed with DI water and stored in DI water at 4 °C. The TFC-LDH membrane was prepared in a similar manner.

The LDH@TFC membrane was prepared by deposition of LDH nanoparticles on PDA-modified TFC membrane as described in our previous work [21]. Briefly, the TFC membrane was first immersed in a PDA Tris buffer solution (2 mg mL^{-1}, pH = 8.5 and 10 mM) at 30 °C for 120 min and afterwards, rinsed with DI-water for 10 s. Consequently, the PDA-modified TFC membrane was immersed in 250 ml Tris buffer solution (pH = 8.5 and 10 mM) containing 0.1 w/v% LDH nanoparticles at 30 °C until desiccation. Finally, the LDH-modified TFC membrane (denoted as LDH@TFC) was rinsed with DI water for another 10 s before use. The LDH-modified TFC-LDH membrane (denoted as LDH@TFC-LDH) was prepared in a similar manner. Fig. 1 illustrated the composition of diverse LDH-based composite membranes, and Table 1 showed key parameters during the preparation of LDH-based composite membranes.

2.5. Evaluation of the composite membranes separation performance

A lab-made cross-flow FO membrane cell was used in the performance experiment. The effective area of the membrane was 11.87 cm^2. 1 M NaCl solution and DI-water were used as the draw solution (DS) and feed solution (FS), respectively. The cross-flow velocity was 0.19 L/min. Obtained composite membranes were tested in two modes: (1) FO mode (feed solution facing the selective layer), and (2) PRO mode (draw solution facing the selective layer). The water flux (J_w, L m^{-2} h^{-1}) and reverse salt flux (J_s, g m^{-2} h^{-1}) of membranes were calculated as follows:

$$J_w = \frac{\Delta V}{A\Delta t} \quad (1)$$

$$J_s = \frac{C_t V_t - C_0 V_0}{A\Delta t} \quad (2)$$

A represented the effective membrane area (m^2); ΔV represented the volume change of DS over a specific time Δt (h); C_0 and V_0 represented

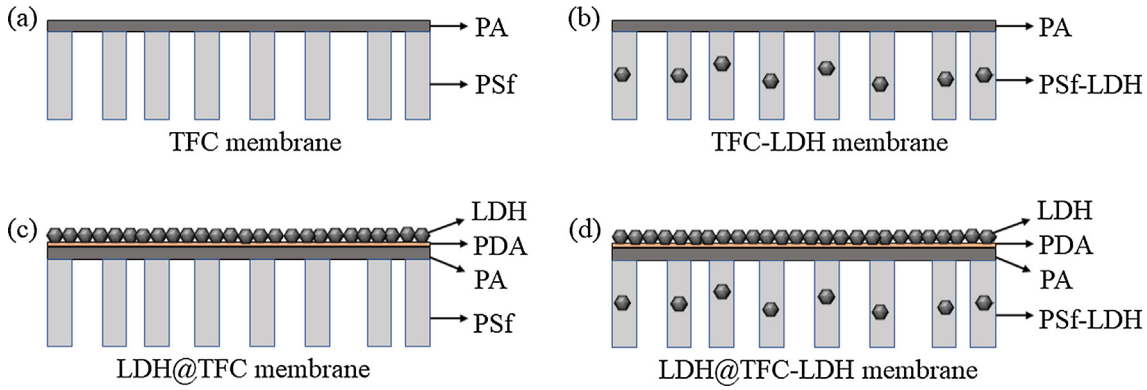

Fig. 1. The composition of composite membranes with different LDHs locations. (a) TFC membrane, (b) TFC-LDH membrane, (c) LDH@TFC membrane and (d) LDH@TFC-LDH membrane.

the initial salt concentration and FS volume, respectively. The salt concentration was measured by an electrical conductivity meter (DDSJ-308F, Shanghai instrument electric science instrument), and C_t and V_t represented their corresponding values at the time t, respectively.

2.6. Evaluation of the chlorine resistance of composite membranes

Chlorine resistance of prepared composite membranes was evaluated under the cross-flow operation in FO mode. 1 M NaCl solution was used as the DS and 1000 ppm NaOCl solution with controlled pH value (4 or 10) was used as the FS. The normalized water flux and reverse salt flux of membranes were employed for evaluating the chlorine resistance.

2.7. Evaluation of the anti-fouling capacity of composite membranes

The anti-fouling capacity of prepared composite membranes was evaluated by fouling tests. The fouling test lasted for 10 h in FO mode and an electronic balance was used to monitor the weight change. The amount of alginate adsorbed ($m_{s,alg}$, mg L^{-1}) during the 10 h fouling experiment was calculated by Livingston et al. [31] with the following equation:

$$m_{s,alg} = \frac{(C_{f,t=0} \times V_{f,t=0}) - (C_{f,t=10} \times V_{f,t=10})}{V_p} \quad (3)$$

C_f and V_f represented the foulant concentration and feed volume before ($t = 0$) and after ($t = 10$) the fouling test, respectively. V_p represented the permeate volume. Initial and final foulant concentrations were measured by a Total Organic Carbon (TOC-V CSH, Shimadzu) analyzer with the non-purgeable organic carbon (NPOC) method.

2.8. Characterization of composite membranes

XRD characterization was carried out on D8 ADVANCE, Bruker. Diffraction patterns were recorded in the range of 2θ = 5–70° with a step size of 0.02°. Attenuated total reflectance flourier transform infrared spectroscopy (ATR-FTIR, VERTEX 70, Bruker) was employed to identify functional groups located on MgAl-CO_3 LDH nanoparticles and composite membranes. Surface and cross-sectional SEM images of prepared membranes were taken by a Nova NanoSEM 450 field emission scanning electron microscope. Before SEM characterization, membranes were freeze-dried and coated with gold nanoparticles using a sputtering coater (MCIOOO ION SPUTTER). Surface roughness was measured using an atomic force microscope (AFM, NanoScope V MultiMode8, Bruker). A tapping mode was operated with images taken in the range of 5 μm × 5 μm. The mean roughness (Ra) was used for membrane surface characterization. Surface hydrophilicity of prepared membranes was evaluated by water contact angle using a contact angle system (DSA100, Krüss). For each type of membrane, three different samples were tested in twelve random locations. Interfacial free energy of the composite membrane was evaluated with the following Eq. (4):

$$-\Delta G_{ML} = \gamma_L \left(1 + \frac{\cos\theta}{1 + SAD}\right) \quad (4)$$

where θ represented the average contact angle, SAD represented the surface area difference obtained from of AFM measurement and γ_L represented the pure water surface tension (72.8 mJ m^{-2} at 25 °C).

3. Results and discussion

3.1. Investigation of the location of LDHs on physicochemical properties of membranes

Fig. 2 illustrated XRD patterns of MgAl-CO_3 LDH nanoparticles, PSf, PSf-LDH, TFC, TFC-LDH, LDH@TFC and LDH@TFC-LDH membranes. As shown in Fig. 2, six characteristic diffraction peaks could be precisely assigned to (0 0 3), (0 0 6), (0 0 9), (0 1 5), (0 1 8) and (110/113) planes of CO_3-intercalated LDH phase, respectively, therefore indicating a high crystallinity and well-developed layered structure [32]. Moreover, no conspicuous difference could be observed between PSf and PSf-LDH substrates in the XRD pattern, suggesting that introduced LDH-nanoparticles were well-dispersed in PSf substrates [6]. In addition, the appearance of a weak diffraction peak located at 11.3°, which could be assigned to the (0 0 3) diffraction plane of the LDH phase,

Table 1
Key parameters during the preparation of LDH-based composite membranes.

Membranes	Casting solution				LDHs modification	
	PSf (g)	NMP (g)	DMF (g)	LDHs (g)	PDA coating (min)	0.1 w/v% LDHs suspension (mL)
TFC	12	66	22	0	0	0
TFC-LDH	12	66	22	0.24	0	0
LDH@TFC	12	66	22	0	120	250
LDH@TFC-LDH	12	66	22	0.24	120	250

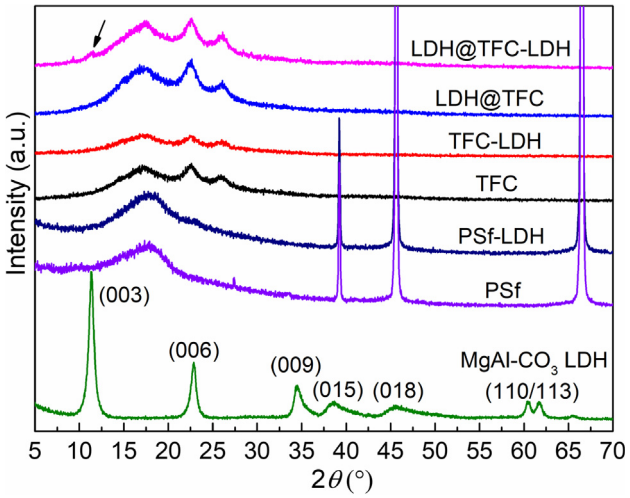

Fig. 2. XRD patterns of the MgAl-CO_3 LDH nanoparticles, PSf, PSf-LDH, TFC, TFC-LDH, LDH@TFC and LDH@TFC-LDH membranes.

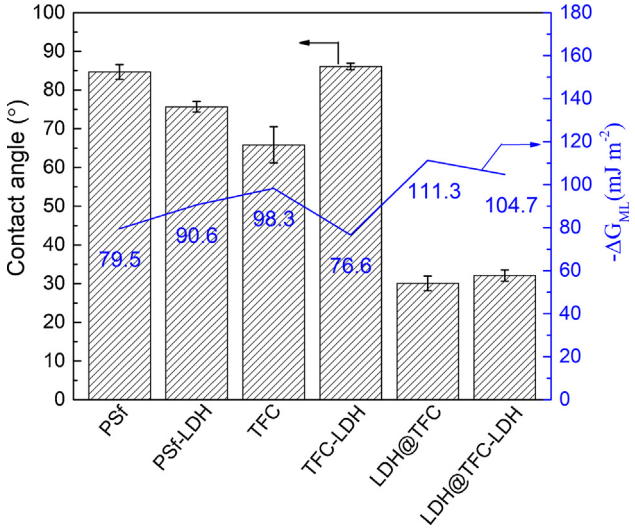

Fig. 3. Contact angles and interfacial free energy analysis of PSf, PSf-LDH, TFC, TFC-LDH, LDH@TFC and LDH@TFC-LDH membranes.

clearly indicated that MgAl-CO_3 LDH nanoparticles retained their crystallinity and interlayer gallery height after deposition on the surface of PA active layers.

Fig. S1 illustrated ATR-FTIR profiles of MgAl-CO_3 LDH nanoparticles, PSf, PSf-LDH, TFC, TFC-LDH, LDH@TFC and LDH@TFC-LDH membranes, respectively. Absorption peaks located at 1151 cm^{-1} and 1293 cm^{-1} could be assigned to the symmetric and asymmetric O═S═O stretching vibrations, respectively; while the absorption peak located at 1240 cm^{-1} could be assigned to asymmetric C—O—C stretching vibration; diffraction peaks located at 1503 cm^{-1} and 1411 cm^{-1} could be assigned to CH_3—C—CH_3 and C═C aromatic ring stretching vibrations, respectively. All these absorption peaks should stem from PSf substrates [33]. It should be emphasized that there existed no significant differences in ATR-FTIR spectra between PSf and PSf-LDH substrates except a characteristic peak at 620 cm^{-1}, which was associated with Al—O and Mg—O vibrations within the LDH phase [33]. After the introduction of PA active layers by interfacial polymerization, both TFC and TFC-LDH membranes exhibited characteristic absorption peaks located at 1662, 1610, and 1541 cm^{-1}, indicating the formation of stable PA active layers on substrates. After deposition of MgAl-CO_3 LDH nanoparticles, characteristic absorption peaks derived from PA active layers were significantly weakened. Moreover, a significant change in the shape of absorption peak located at 1370 cm^{-1} could be ascribed to the interference from carbonate anions located in interlayer galleries of MgAl-CO_3 LDH nanoparticles. All these results strongly supported that MgAl-CO_3 LDH nanoparticles had been firmly attached to the PA active layer surface and evenly blended with the PSf substrate, respectively.

To investigate the influence of LDH nanoparticles on surface hydrophilicity of composite membranes, the water contact angle and interfacial free energy of PSf, PSf-LDH, TFC, TFC-LDH, LDH@TFC and LDH@TFC-LDH membranes were further measured (shown in Fig. 3). In addition, considering the significant influence of surface roughness of composite membranes on their surface hydrophilicity, AFM characterization was further conducted to determine their surface average roughness (Ra) (Fig. S2) and SAD value. It was observed that the contact angle of the PSf substrate was decreased from 85° to 75° after the addition of hydrophilic LDH nanoparticles. Simultaneously, the interfacial free energy, which was calculated based on Eq. (4), was increased from 79.5 mJ m^{-2} to 90.6 mJ m^{-2}, therefore indicating that incorporation of LDH nanoparticles had effectively improved the surface wettability of pristine PSf substrates [6]. After coating the PSf substrate with a PA active layer, the contact angle reached 65° due to the intrinsic hydrophilicity of the PA phase. Nevertheless, compared with pristine TFC membrane, contact angle of the TFC-LDH membrane further increased to 85°, which was attributed to the increased surface roughness (Fig. S2d) and larger grain size (Fig. S3b). After deposition of LDHs, contact angles of LDH@TFC and LDH@TFC-LDH membranes significantly reduced to 30° and 32°, respectively, owing to the intrinsic hydrophilicity of MgAl-CO_3 LDH nanoparticles. It was therefore deduced that increasing the surface hydrophobicity via LDH nanoparticle modification should be beneficial for improving the water flux of TFC membranes. In addition, since there existed a strong hydration layer on a highly hydrophilic surface, anti-fouling capacity of the LDH-modified TFC membrane was anticipated to be improved [34].

3.2. Investigation of the effect of LDH location on the membrane microstructure

Fig. S4 presented top and cross-sectional SEM images of PSf and PSf-LDH substrates, respectively. It was observed that incorporation of LDH nanoparticles induced slight changes in the surface morphology of substrates. Top SEM images indicated that the surface porosity became higher upon incorporation of LDH nanocrystals into the PSf substrate (Fig. S4b). Cross-sectional SEM images further indicated that after blending with LDH nanoparticles, a well-interconnected pore architecture was generated within the substrate (shown in Fig. S4c and d). This morphological change could be explained by delayed de-mixing induced by incorporation of hydrophilic LDH nanoparticles during the phase separation process [6,33]. It was believed that improvements in both porosity and pore structure favored the reduction of water permeation barrier [35].

Fig. S3 showed top views of four types of composite membranes with different LDH locations. The pristine TFC membrane showed a typical “ridge-valley” morphology [7,21,22,36]. After blending with LDHs, grain size of the TFC-LDH membrane became larger. Surface deposition of LDH nanoparticles led to smoother surface morphology. In comparison, LDH nanoparticles were more densely packed on the LDH@TFC-LDH membrane (shown in Fig. S3d), which was beneficial for improving the chlorine resistance and anti-fouling capacity.

3.3. Investigation of the influence of LDH locations on the osmosis performance of composite membranes

Fig. 4 showed the separation performance of prepared composite membranes with different LDH locations in both FO and PRO modes. In the FO mode, water flux of pristine TFC membrane reached

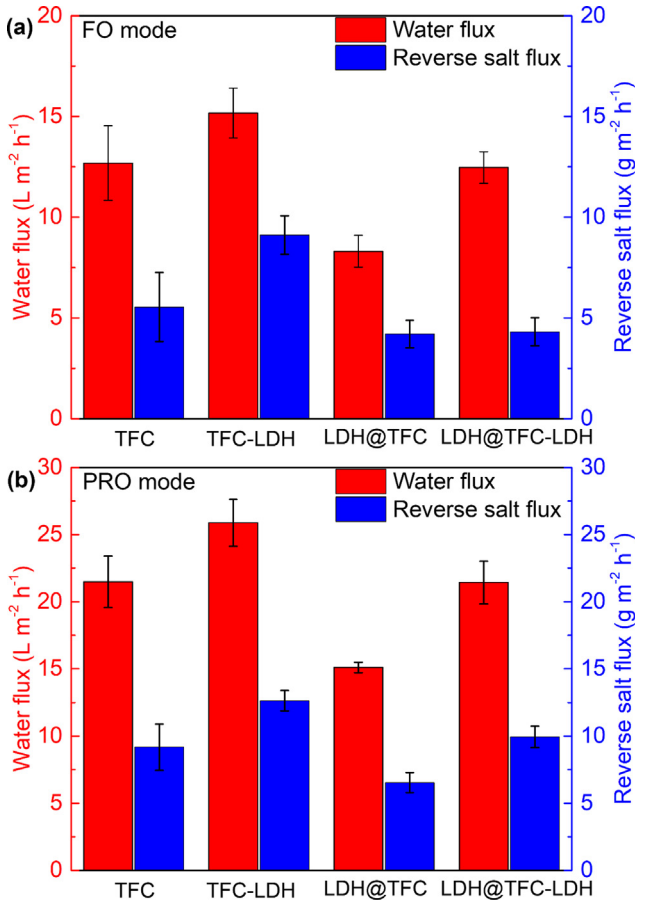

Fig. 4. Performance of membranes with different LDHs location. (a) Forward osmosis (FO) mode (FS facing the selective layer), and (b) Pressure retarded osmosis (PRO) mode (DS facing the selective layer). Operating conditions: 1 M NaCl as draw solution and DI-water as the feed solution, each test was conducted for 1 h in triplicate.

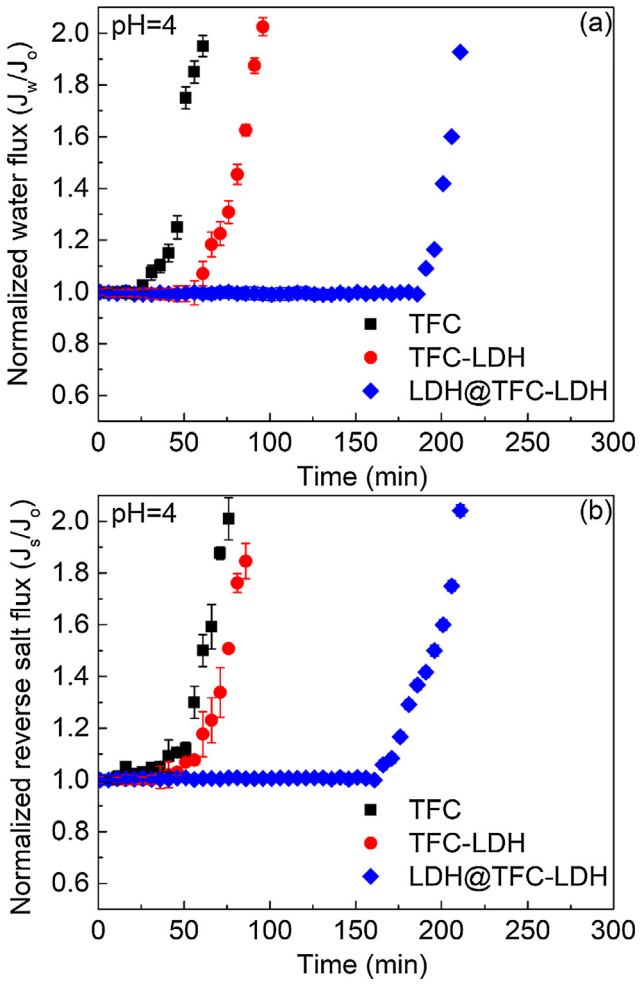

Fig. 5. The normalized water flux (a) and reverse salt flux (b) of composite membranes tested in FO mode (FS facing the selective layer). Operating conditions: 1 M NaCl as draw solution, 1000 ppm NaOCl aqueous solution as feed solution and 1 M HCl used to adjust pH value was 4.

12.6 L m^{-2} h^{-1}, and the reverse salt flux reached 5.6 g m^{-2} h^{-1}. After blending with LDH nanoparticles, the water flux of TFC-LDH membrane significantly increased from 12.6 L m^{-2} h^{-1} to 15.2 L m^{-2} h^{-1} in the FO mode and from 21.5 L m^{-2} h^{-1} to 25.9 L m^{-2} h^{-1} in the PRO mode. The significantly enhanced water flux could be attributed to higher porosity and well-interconnected pore architecture of the PSf-LDH substrate, which effectively alleviated the undesired ICP effect [3,6]. In contrast, both water flux and reverse salt flux of the LDH@TFC membrane were remarkably reduced in both FO and PRO modes possibly due to the higher hydraulic resistance [21]. In the case of LDH@TFC-LDH membranes, the water flux again reached 12.5 L m^{-2} h^{-1} and 21.4 L m^{-2} h^{-1} in FO and PRO modes respectively, which were close to that of pristine TFC membrane. This could be attributed to the trade-off effect of LDH nanoparticles in different locations. In addition, the reverse salt flux of the LDH@TFC-LDH membrane was comparable with the pristine TFC membrane. A detailed performance comparison with other TFC FO membranes as reported in the literature was listed in Table 2.

3.4. Investigation of the chlorine resistance of composite membranes

Chemical cleaning with NaOCl represents a facile and economical approach to alleviate the membrane fouling. When compared with pressure-driven processes, e.g. RO, the fouling of FO membranes is less

Table 2
A summary of the performance of commercial FO membranes.

Membranes	FO mode		PRO mode		Test condition	References
	J_w	J_s	J_w	J_s		
TFC	12.6	5.6	21.5	9.2	1 M NaCl as draw, DI-water as feed	This work
TFC-LDH	15.2	9.2	25.9	12.6	1 M NaCl as draw, DI-water as feed	This work
LDH@TFC	8.3	4.2	15.1	6.5	1 M NaCl as draw, DI-water as feed	This work
LDH@TFC-LDH	12.5	4.3	21.4	9.9	1 M NaCl as draw, DI-water as feed	This work
HTI TFC	18.5	6.7	44	11	2 M NaCl as draw, DI-water as feed	[36]
Oasys Water TFC	20	–	50	–	1.5 M NaCl as draw, DI-water as feed	[38]
HTI TFC	15.1	4.4	–	–	1 M NaCl as draw, DI-water as feed	[39]
HTI TFC	~8.5	~6	~21	~12	1 M NaCl as draw, DI-water as feed	[40]

severe and can be cleaned more efficiently. However, membrane fouling remains a great challenge in FO, and NaOCl cleaning is required in case a highly contaminated FS is used. Herein the anti-chlorination properties of TFC, TFC-LDH and LDH@TFC-LDH membranes were further evaluated in the FO mode. Chlorine resistance tests were conducted under both acidic (pH = 4) and alkaline (pH = 10) conditions [10,11]. Fig. 5 showed the effect of LDHs locations on the separation performance of prepared TFC membranes after chlorination at pH = 4. It was observed that the water flux and reverse salt flux of composite membranes were significantly changed upon exposure to 1000 ppm NaOCl solution. Notably, water flux and reverse salt flux of TFC membranes quickly increased twice within 75 min, which could be attributed to irreversible degradation of the PA active layer as was observed in previous studies [10,21]. In contrast, both water flux and reverse salt flux of the TFC-LDH membrane remained unchanged within 50 min in case LDH nanoparticles were incorporated into the PSf substrate, owing to the relatively larger grain size of the PA active layer (shown in Fig. S3b). Moreover, both water flux and reverse salt flux of the LDH@TFC-LDH membrane was stable within the exposure time of 210 min, therefore confirming that surface deposition of LDH nanoparticles (see Fig. S3d) had effectively protected the PA active layer from the nucleophilic attack of active chlorine species [21].

Anti-chlorination properties of TFC, TFC-LDH and LDH@TFC-LDH membranes upon exposure to 1000 ppm NaOCl solution at pH = 10 were shown in Fig. 6. Results showed that the water flux and reverse salt flux of both TFC and TFC-LDH membranes followed the same trend as in the case of pH = 4. Nevertheless, the increase rate slowed down since hypochlorite anions (OCl^-) instead of hypochlorous acid (HOCl), which were considered more oxidative, became dominant species as the pH value increased from 4 to 10 [10]. In contrast, the LDH@TFC-LDH membrane remained stable even upon exposure to NaOCl solution for 5 h at pH = 10. As shown in Fig. 6(a), a gradual decrease in the water flux of the LDH@TFC-LDH membrane with the prolongation of exposure time could be attributed to unavoidable dilution of the DS. To summarize, the above results clearly indicated that LDH@TFC-LDH membranes exhibited excellent chlorine resistance, owing to the unique barrier effect of post-modified LDH nanoparticles.

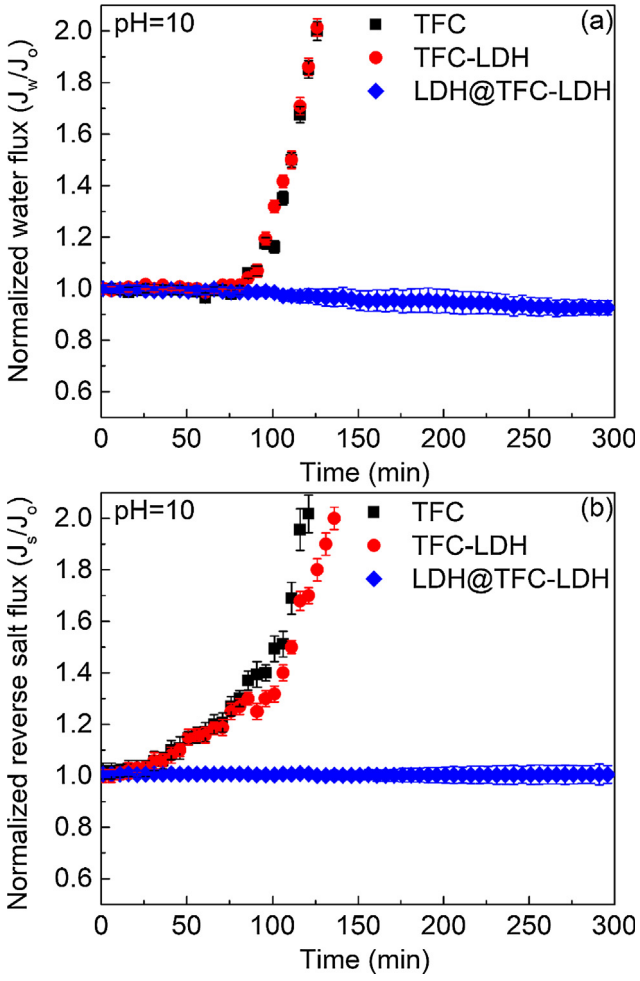

Fig. 6. (a) Normalized water flux and (b) reverse salt flux of composite membranes tested in FO mode (FS facing the selective layer). Operating conditions: 1 M NaCl as draw solution, 1000 ppm NaOCl aqueous solution as feed solution and 1 M NaOH used to adjust the pH value to 10.

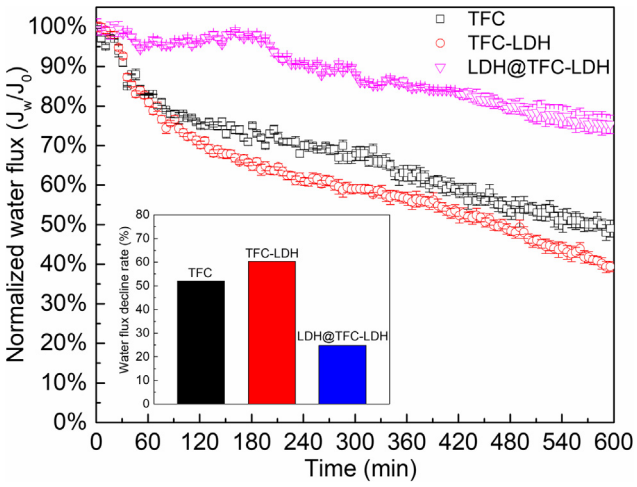

Fig. 7. The normalized water flux of composite membranes tested in FO mode (FS facing the selective layer) in the presence of 200 mg L^{-1} sodium alginate, 50 mM NaCl, and 0.5 mM $CaCl_2$. Operating conditions: 2 M NaCl was used as draw solution, each test was conducted for 10 h in triplicate.

3.5. Investigation of the anti-fouling capacity of composite membranes

Fig. 7 illustrated the normalized water flux decline of TFC, TFC-LDH and LDH@TFC-LDH membranes due to organic fouling on the membrane surface. The effective flux was plotted as a function of the fouling time. The pristine TFC membrane retained ~50% of its initial water flux after runing for 10 h, owing to the irreversible alginate fouling in the presence of $CaCl_2$, which was known as the bridging effect caused by calcium ions [37]. In contrast, the TFC-LDH membrane retained only ~40% of its initial water flux in the FO mode, which was attributed to the higher water flux (15.2 L m^{-2} h^{-1}) and surface roughness (Ra = 132 nm). These factors aggravated the preferential adhesion of pollutants on the membrane surface [37]. In contrast, the LDH@TFC-LDH membrane retained ~75% of the initial water flux. The significantly improved anti-fouling capacity could be attributed to the enhanced surface hydrophilicity caused by surface deposition of LDH nanoparticles (Fig. 3), which effectively alleviated the preferential adsorption of alginate onto the membrane surface. Table 3 showed the specific mass of alginate adsorbed on different composite membrane surface. It was found that the LDH@TFC-LDH membrane exhibited the least adsorbed mass towards alginate (2.5 mg L^{-1}), which was

Table 3
Effect of the type of composite membranes on the specific mass of alginate adsorbed during fouling.

Membranes	Modes	Specific mass of alginate adsorbed (mg L^{-1})
TFC	FO mode	9.6
TFC-LDH	FO mode	11.9
LDH@TFC-LDH	FO mode	2.5

consistent with the trend in water flux decline.

4. Conclusions

In this study, LDH nanoparticles were incorporated in the pristine TFC membrane to improve the chlorine resistance and anti-fouling capacity. Results showed that simultaneous depositing LDH nanoparticles on the PA active layer and blending the PSf substrate with LDH nanoparticles were beneficial for enhancing the chlorine resistance at pH = 10 without sacrificing the water flux in comparison with the pristine TFC membrane. At pH = 4, both water flux and reverse salt flux of the LDH@TFC-LDH membrane remained stable within 210 min. Prepared LDH@TFC-LDH membranes were highly promising for mass production, owing to the low manufacturing cost of LDH nanoparticles [24] and the simple manufacturing process. Once fouled, prepared LDH@TFC-LDH membranes could be quickly and easily recovered. Further research should be conducted on enhancing the LDH@TFC-LDH membrane stability under acid conditions.

Acknowledgements

This work was supported by the National Natural Science Foundation of China (21622607, 21176231, 21761132009), the Thousand Youth Talents Program, the Zhejiang Provincial Natural Science Foundation (LQ19E080005), and K.C. Wong Magna Fundation in Ningbo University.

Appendix A. Supplementary material

Supplementary data to this article can be found online at https://doi.org/10.1016/j.seppur.2019.03.039.

References

[1] X.J. Song, L. Wang, L.L. Mao, Z.N. Wang, Nanocomposite membrane with different carbon nanotubes location for nanofiltration and forward osmosis applications, ACS Sustain. Chem. Eng. 4 (2016) 2990–2997.
[2] W.X. Xu, Q.Z. Chen, Q.C. Ge, Recent advances in forward osmosis (FO) membrane: chemical modifications on membranes for FO processes, Desalination 419 (2017) 101–116.
[3] M. Rastgar, A. Bozorg, A. Shakeri, Novel dimensionally controlled nanopore forming template in forward osmosis membranes, Environ. Sci. Technol. 52 (2018) 2704–2716.
[4] V. Sant'Anna, L.D.F. Marczak, I.C. Tessaro, Membrane concentration of liquid foods by forward osmosis: process and quality view, J. Food Eng. 111 (2012) 483–489.
[5] D. Zhao, G. Qiu, X. Li, C. Wan, K. Lu, T.S. Chung, Zwitterions coated hollow fiber membranes with enhanced antifouling properties for osmotic power generation from municipal wastewater, Water Res. 104 (2016) 389–396.
[6] P. Lu, S. Liang, L. Qiu, Y.S. Gao, Q. Wang, Thin film nanocomposite forward osmosis membranes based on layered double hydroxide nanoparticles blended substrates, J. Membr. Sci. 504 (2016) 196–205.
[7] Z.Z. Zhou, J.Y. Lee, T.S. Chung, Thin film composite forward-osmosis membranes with enhanced internal osmotic pressure for internal concentration polarization reduction, Chem. Eng. J. 249 (2014) 236–245.
[8] S.A.F. Zhao, L.D. Zou, Relating solution physicochemical properties to internal concentration polarization in forward osmosis, J. Membr. Sci. 379 (2011) 459–467.
[9] W.D. Ding, Y.M. Li, M.T. Bao, J.R. Zhang, C.C. Zhang, J.R. Lu, Highly permeable and stable forward osmosis (FO) membrane based on the incorporation of Al_2O_3 nanoparticles into both substrate and polyamide active layer, RSC Adv. 7 (2017) 40311–40320.
[10] T.P.N. Nguyen, B.M. Jun, Y.N. Kwon, The chlorination mechanism of integrally asymmetric cellulose triacetate (CTA)-based and thin film composite polyamide-based forward osmosis membrane, J. Membr. Sci. 523 (2017) 111–121.
[11] P. Xie, C.F. de Lannoy, J. Ma, Z. Wang, S. Wang, J. Li, M.R. Wiesner, Improved chlorine tolerance of a polyvinyl pyrrolidone-polysulfone membrane enabled by carboxylated carbon nanotubes, Water Res. 104 (2016) 497–506.
[12] B.X. Mi, M. Elimelech, Organic fouling of forward osmosis membranes: fouling reversibility and cleaning without chemical reagents, J. Membr. Sci. 348 (2010) 337–345.
[13] J. Xu, Z. Wang, L.L. Yu, J.X. Wang, S.C. Wang, A novel reverse osmosis membrane with regenerable anti-biofouling and chlorine resistant properties, J. Membr. Sci. 435 (2013) 80–91.
[14] D. Emadzadeh, W.J. Lau, T. Matsuura, M. Rahbari-Sisakht, A.F. Ismail, A novel thin film composite forward osmosis membrane prepared from PSf–TiO_2 nanocomposite substrate for water desalination, Chem. Eng. J. 237 (2014) 70–80.
[15] X. Liu, H.Y. Ng, Fabrication of layered silica–polysulfone mixed matrix substrate membrane for enhancing performance of thin-film composite forward osmosis membrane, J. Membr. Sci. 481 (2015) 148–163.
[16] N. Ma, J. Wei, R.H. Liao, C.Y. Tang, Zeolite-polyamide thin film nanocomposite membranes: towards enhanced performance for forward osmosis, J. Membr. Sci. 405 (2012) 149–157.
[17] Y.P. Tang, J.X. Chan, T.S. Chung, M. Weber, C. Staudt, C. Maletzko, Simultaneously covalent and ionic bridging towards antifouling of GO-imbedded nanocomposite hollow fiber membranes, J. Mater. Chem. A 3 (2015) 10573–10584.
[18] S. Manzeli, D. Ovchinnikov, D. Pasquier, O.V. Yazyev, A. Kis, 2D transition metal dichalcogenides, Nat. Rev. Mater. 2 (2017) 17033.
[19] J. Zhu, L. Qin, A. Uliana, J. Hou, J. Wang, Y. Zhang, X. Li, S. Yuan, J. Li, M. Tian, J. Lin, B. Van der Bruggen, Elevated performance of thin film nanocomposite membranes enabled by modified hydrophilic MOFs for nanofiltration, ACS Appl. Mater. Interfaces 9 (2017) 1975–1986.
[20] P. Anadao, L.F. Sato, H. Wiebeck, F.R. Valenzuela-Diaz, Montmorillonite as a component of polysulfone nanocomposite membranes, Appl. Clay Sci. 48 (2010) 127–132.
[21] P. Lu, S. Liang, T.T. Zhou, T.S. Xue, X.Y. Mei, Q. Wang, Layered double hydroxide nanoparticle modified forward osmosis membranes via polydopamine immobilization with significantly enhanced chlorine and fouling resistance, Desalination 421 (2017) 99–109.
[22] M.J. Park, S. Phuntsho, T. He, G.M. Nisola, L.D. Tijing, X.M. Li, G. Chen, W.J. Chung, H.K. Shon, Graphene oxide incorporated polysulfone substrate for the fabrication of flat-sheet thin-film composite forward osmosis membranes, J. Membr. Sci. 493 (2015) 496–507.
[23] S. Morales-Torres, C.M.P. Esteves, J.L. Figueiredo, A.M.T. Silva, Thin-film composite forward osmosis membranes based on polysulfone supports blended with nanostructured carbon materials, J. Membr. Sci. 520 (2016) 326–336.
[24] P. Lu, Y. Liu, T. Zhou, Q. Wang, Y. Li, Recent advances in layered double hydroxides (LDHs) as two-dimensional membrane materials for gas and liquid separations, J. Membr. Sci. 567 (2018) 89–103.
[25] Q. Wang, H.H. Ay, Z.Y. Zhong, J.Z. Luo, A. Borgna, Synthesis of high-temperature CO_2 adsorbents from organo-layered double hydroxides with markedly improved CO_2 capture capacity, Energy Environ. Sci. 5 (2012) 7526–7530.
[26] Z.P. Wang, P. Lu, X.M. Zhang, L.G. Wang, Q. Li, Z.L. Zhang, NOx storage and soot combustion over well-dispersed mesoporous mixed oxides via hydrotalcite-like precursors, RSC Adv. 5 (2015) 52743–52753.
[27] Y.S. Gao, J.W. Wu, Q. Wang, C.A. Wilkie, D. O'Hare, Flame retardant polymer/layered double hydroxide nanocomposites, J. Mater. Chem. A 2 (2014) 10996–11016.
[28] J. Wang, T. Zhang, M. Li, Y. Yang, P. Lu, P. Ning, Q. Wang, Arsenic removal from water/wastewater using layered double hydroxide derived adsorbents, a critical review, RSC Adv. 8 (2018) 22694–22709.
[29] A.C.S. Alcântara, P. Aranda, M. Darder, E. Ruiz-Hitzky, Bionanocomposites based on alginate–zein/layered double hydroxide materials as drug delivery systems, J. Mater. Chem. 20 (2010) 9495–9504.
[30] Q. Wang, D. O'Hare, Large-scale synthesis of highly dispersed layered double hydroxide powders containing delaminated single layer nanosheets, Chem. Commun. (Camb) 49 (2013) 6301–6303.
[31] N.M. Mazlan, P. Marchetti, H.A. Maples, B. Gu, S. Karan, A. Bismarck, A.G. Livingston, Organic fouling behaviour of structurally and chemically different forward osmosis membranes – a study of cellulose triacetate and thin film composite membranes, J. Membr. Sci. 520 (2016) 247–261.
[32] J. Wang, Y. Yang, L. Jia, N. Yang, Q. Guan, L. Huang, A. Umar, Q. Wang, P. Ning, The influence of the charge compensating anions of layered double hydroxides (LDHs) in LDH-NS/graphene oxide nanohybrid for CO_2 capture, J. Nanosci. Nanotechnol. 18 (2018) 2956–2964.
[33] P. Lu, S. Liang, T.T. Zhou, X.Y. Mei, Y. Zhang, C. Zhang, Q. Wang, Layered double hydroxide/graphene oxide hybrid incorporated polysulfone substrate for thin-film nanocomposite forward osmosis membranes, RSC Adv. 6 (2016) 56599–56609.
[34] S. Liang, G.G. Qi, K. Xiao, J.Y. Sun, E.P. Giannelis, X. Huang, M. Elimelech, Organic fouling behavior of superhydrophilic polyvinylidene fluoride (PVDF) ultrafiltration membranes functionalized with surface-tailored nanoparticles: Implications for organic fouling in membrane bioreactors, J. Membr. Sci. 463 (2014) 94–101.
[35] N. Ma, J. Wei, S.R. Qi, Y. Zhao, Y.B. Gao, C.Y. Tang, Nanocomposite substrates for controlling internal concentration polarization in forward osmosis membranes, J. Membr. Sci. 441 (2013) 54–62.
[36] G. Han, B.W. Zhao, F.J. Fu, T.S. Chung, M. Weber, C. Staudt, C. Maletzko, High performance thin-film composite membranes with mesh-reinforced hydrophilic sulfonated polyphenylenesulfone (sPPSU) substrates for osmotically driven processes, J. Membr. Sci. 502 (2016) 84–93.
[37] Y.N. Wang, E. Jarvela, J. Wei, M.M. Zhang, H. Kyllonen, R. Wang, C.Y. Tang, Gypsum scaling and membrane integrity of osmotically driven membranes: the effect of membrane materials and operating conditions, Desalination 377 (2016) 1–10.
[38] J.T. Arena, S.S. Manickam, K.K. Reimund, P. Brodskiy, J.R. McCutcheon, Characterization and performance relationships for a commercial thin film composite membrane in forward osmosis desalination and pressure retarded osmosis, Ind. Eng. Chem. Res. 54 (2015) 11393–11403.
[39] J. Ren, J.R. McCutcheon, A new commercial thin film composite membrane for forward osmosis, Desalination 343 (2014) 187–193.
[40] M.R. Chowdhury, L.W. Huang, J.R. McCutcheon, Thin film composite membranes for forward osmosis supported by commercial nanofiber nonwovens, Ind. Eng. Chem. Res. 56 (2017) 1057–1063.